

University of Nebraska - Lincoln

DigitalCommons@University of Nebraska - Lincoln

Papers in Natural Resources

Natural Resources, School of

2003

Air Temperature Errors Caused by Air Filter and Construction Effects on HMP45C Temperature Sensors in Weather Stations

K. G. Hubbard

University of Nebraska, Lincoln, Nebraska, khubbard1@unl.edu

X Lin

University of Nebraska, Lincoln, Nebraska, xiaomao.csi@gmail.com

Follow this and additional works at: <https://digitalcommons.unl.edu/natrespapers>



Part of the [Natural Resources and Conservation Commons](#)

Hubbard, K. G. and Lin, X, "Air Temperature Errors Caused by Air Filter and Construction Effects on HMP45C Temperature Sensors in Weather Stations" (2003). *Papers in Natural Resources*. 215.
<https://digitalcommons.unl.edu/natrespapers/215>

This Article is brought to you for free and open access by the Natural Resources, School of at DigitalCommons@University of Nebraska - Lincoln. It has been accepted for inclusion in Papers in Natural Resources by an authorized administrator of DigitalCommons@University of Nebraska - Lincoln.

AIR TEMPERATURE ERRORS CAUSED BY AIR FILTER AND CONDUCTION EFFECTS ON HMP45C TEMPERATURE SENSORS IN WEATHER STATIONS

K. G. Hubbard, X. Lin

ABSTRACT. For non-ventilated air temperature measurements at weather stations, both ambient wind speed and solar radiation are known to affect the magnitude of air temperature measurement errors. The objective of this study is to explore the effect of the sensor's housing and to quantify any stagnation or conduction errors. The HMP45C temperature and relative humidity sensor with a Gill radiation shield is widely used in remote monitoring sites. The use of a filter in the HMP45C leads to loss of ventilation, while the protrusion of the sensor housing below the Gill shield exposes it to radiation loading and potentially increased conduction of heat to the sensor. The HMP45C sensors were deployed with and without an air filter in both standard Gill shields and in a Gill shield modified with extra plates to completely cover the base of the sensor housing. The data collected were examined using spectral analysis and statistical methods. Results show that both average air temperature errors and variations of air temperature errors were smaller in the HMP45C sensors when the manufacturer-supplied air filter was removed. The ranges of the three-sigma errors can be decreased by 0.4 °C to 0.7 °C and the accuracy of monthly average air temperature can be improved at least 0.1 °C by employing an HMP45C without the air filter. Results suggest that the maximum air temperature taken with the filter may reach more than 1.0 °C higher than that taken without the filter. The major frequency component contributing to air temperature errors using the HMP45C sensor in the Gill shield is the frequency of one day per cycle, which is expected. Partial radiation blocking combined with aspiration significantly reduces the contribution of the one-day cycle. In field tests, the R. M. Young aspirated temperature system proved very accurate compared to an aspirated precision industrial platinum resistance thermometer (PRT).

Keywords. Air filter, Air temperature error, Spectral analysis, Wavelet transforms.

HMP45C temperature sensors (Campbell Scientific, Logan, Utah) are widely used in operational weather station networks and in monitoring efforts associated with research. The HMP45C temperature and relative humidity sensor contains a platinum resistance temperature detector (PRT) and a Vaisala HUMICAP® 180 capacitive-type relative humidity sensor. For air temperature measurement, the HMP45C sensor is usually housed in a Gill radiation shield to reduce the radiation errors and protect the temperature sensor from inclement weather. The HMP45C sensor head is relatively simple in design with an air filter (double-fold black filter) that encloses the temperature and relative humidity sensing elements (fig. 1). This filter consists of an outer slatted black screen cap, a 0.2 µm pore Teflon membrane, and an inner slatted black screen cap. The primary function of this air filter

is to protect the relative humidity sensor from dust and chemical pollutants while allowing air molecules to move freely and diffusely through the filter and past the sensing elements located inside.

For non-ventilated air temperature measurements in field or weather stations, both the ambient wind speed (Lin et al., 2001a) and the solar radiation (Hubbard et al., 2001; Lin et al., 2001b) are linked to the magnitude of air temperature measurement errors. However, for the HMP45C sensor with the Gill shield system, an additional and potentially serious source of error in measurements is the use of a double-fold black filter, which isolates the temperature sensing element from the moving air stream (air speed inside the filter is close to zero due to the diffuse properties of the air filter). Sufficient air movement past the sensor is necessary to maintain thermal equilibrium between the sensing element and the air, thereby allowing accurate representation of air temperature in real time (Lin, 1999; Lin et al., 2001b).

Simultaneously, the outer black screen cap absorbs most of the incident radiation energy (solar and infrared). The source of this radiation energy is emission from the inner surfaces of the radiation shield or the solar irradiance entering, after multiple reflections, through the Gill shield (Hubbard et al., 2001). The air filter temperature is therefore different from the sensing element temperature, resulting in unbalanced infrared energy (an error source for air temperature measurement). At times, the Gill shield does not provide sufficient ventilation for the temperature sensor (Brock et al., 1995; Lin, 1999; Lin et al., 2001a). This HMP45C filter

Article was submitted for review in November 2001; approved for publication by the Structures & Environment Division of ASAE in January 2003. This article has been approved as Journal Series No. 13208 by the Agricultural Research Division, University of Nebraska-Lincoln. Mention of specific trade names is for reference only and does not imply exclusion of others that may be suitable.

The authors are **Kenneth G. Hubbard**, Professor, and **Xiaomao Lin**, Research Assistant Professor; School of Natural Resource Sciences, University of Nebraska, Lincoln, Nebraska. **Corresponding author:** Dr. Kenneth G. Hubbard, School of Natural Resource Sciences, 244 L.W. Chase Hall, University of Nebraska, Lincoln, NE 68583-0728; phone: 402-472-8294; fax: 402-472-6614; e-mail: khubbard1@unl.edu.

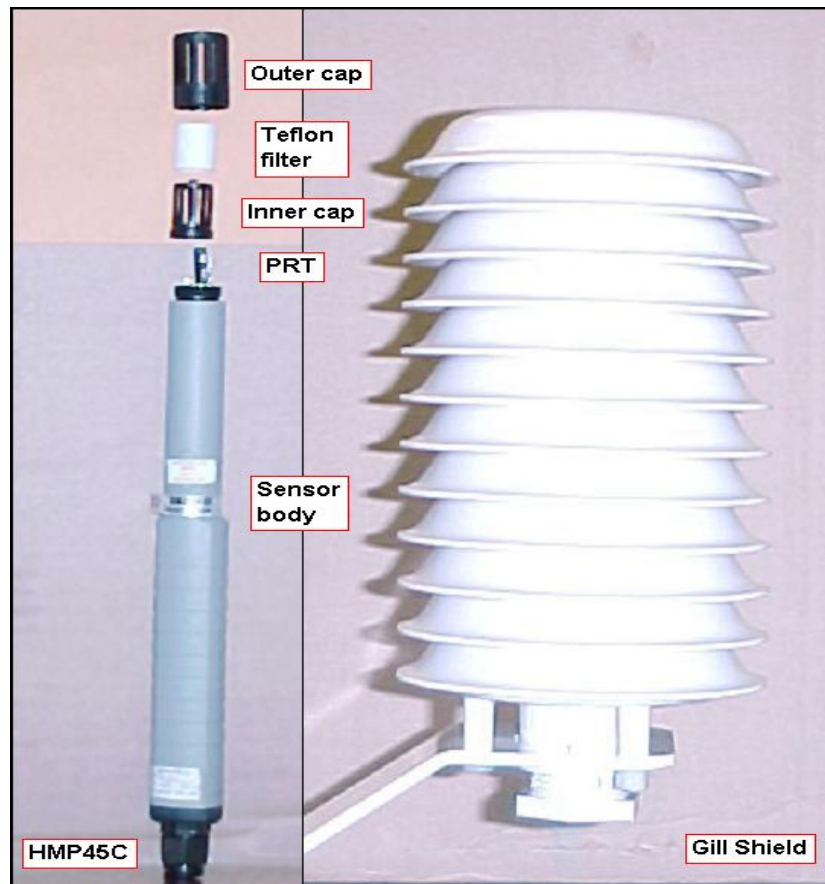


Figure 1. HMP45C sensor and Gill radiation shield.

configuration may further degrade ventilation and increase the radiation effects on the air temperature sensing element located inside the Gill shield.

Another possible source of error for the HMP45C is thermal conduction due to the fact that the sensor housing does not fit completely inside the Gill shield. The exposed portion of the sensor housing may experience high solar irradiance, cold rainwater, and nighttime condensation. This leads us to question whether or not there is significant undesirable conduction of heat to or from the exposed portion of the HMP45C sensor.

Although many air temperature measurements are taken by the HMP45C and Gill shield in field and weather stations, there are a few aspirated air temperature systems applied in the field. The R. M. Young 43347 temperature probe with an aspirated radiation shield (model 43408–L, R. M. Young, Traverse City, Mich.) is a common system that provides better performances (probe accuracy $\pm 0.1^\circ\text{C}$; shield radiation error $< 0.2^\circ\text{C}$ under 1100 W m^{-2} irradiance) because the air sampling flow passing through the sensing element of the temperature probe can reach 3 to 7 m s^{-1} , and the radiation shield consists of double concentric cylinders. We refer to the combination of an R. M. Young 43347 probe and an R. M. Young 43408 radiation shield as the RMY system.

The primary goal of this study was to evaluate the air filter and heat conduction effects on HMP45C sensor readings when the sensor was enclosed in the Gill shield in the field relative to an aspirated precision industrial PRT system. The secondary goal of this study was to evaluate the aspirated RMY air temperature system in the field. To accomplish the

above goals, the following specific objectives were identified:

- Investigate the air filter heating/cooling effects on the air temperature error of the HMP45C sensor.
- Experimentally determine whether or not conduction of heat along the exposed portion of the HMP45C sensor significantly changes temperature in the field.
- Evaluate the RMY system in comparison to an aspirated precision industrial PRT system in the field.

EXPERIMENTAL DESIGN AND DATA ANALYSIS

FIELD MEASUREMENT

Experiments were conducted at the University of Nebraska's Horticulture Experimental Site ($40^\circ 83' \text{ N}$, $96^\circ 67' \text{ W}$, altitude 383 m) located in Lincoln, Nebraska. The site has flat terrain with a surface of mowed grass. One single Gill shield was selected to house the HMP45C sensor with the air filter (double-fold black filter) in place (fig. 1). We refer to this as the single Gill shield with the HMP45C and filter (SWF). The HMP45C sensor without the air filter was placed in a second single Gill shield (SWOF). The third Gill shield was used as a backup with the same combination as the first (SWF).

In order to investigate the effect of conduction errors on air temperature measurements, we simply added plates to a Gill shield until the entire HMP45C sensor housing fit inside with no exposure except for the cable. We refer to this shield as the double Gill shield. Two double Gill shields were used

to mount two HMP45C sensors, one with the filter (DWF) and the other without the filter (DWO). All HMP45C sensors in this study were new probes directly from the manufacturer, and all Gill radiation shields and HMP45C sensors were placed on one A-frame (1.5 m in height) with 70 cm separation. One RMY system was established about 10 m from the A-frame to measure the air temperature at the same height and over the same ground surface. All temperature measurements were taken using a CR10X datalogger (Campbell Scientific, Logan, Utah).

A precision industrial PRT probe (model 5612, Hart Scientific, American Fork, Utah), calibrated by the manufacturer, is NIST traceable. The accuracy of the precision industrial PRT probe is better than $\pm 0.019^\circ\text{C}$ over the range -196°C to $+200^\circ\text{C}$. The temperature measurement of the precision industrial PRT probe was taken using a Tweener thermometer (model 1502A, Hart Scientific). The NIST traceable accuracy of the Tweener thermometer is better than $\pm 0.009^\circ\text{C}$ over the range -100°C to $+100^\circ\text{C}$. Therefore, the total accuracy of the system composed of the Tweener and precision industrial PRT probe should be less than $\pm 0.028^\circ\text{C}$, even assuming that the propagation error in this system is additive. The geometrical dimension of the precision industrial PRT probe was the same as that of the R. M. Young 43347 probe. Thus, an air temperature system was constructed by installing the precision industrial PRT probe into the R. M. Young 43408 radiation shield. It was mounted at the same height as the HMP45C sensors on the A-frame. This system (we call the Tweener system) should be a suitable reference for air temperature measurements in the field because both the temperature sensor and the aspirated radiation shield provide superior performance, as discussed above. Data output from the Tweener system was provided by an RS-232 port. A simple communication program was developed to collect real-time temperature readings on a desktop computer housed in an experimental trailer at some distance from the A-frame. The Tweener system served as a reference for the experiment against which the HMP45C systems and the RMY system were compared.

DATA COLLECTION AND ANALYSIS

Data were collected continuously during the period 10 June to 15 August 2000. Data sampling frequency was 0.1

Hz (10 s), and signals were averaged over 5-min outputs. To avoid possible inherent bias of the HMP45C sensor in a fixed single shield or double shield, the HMP45C sensors were interchanged after the first month. Thus, two one-month periods were available for analysis. The air temperature error was defined as the difference between the air temperatures measured by HMP45C sensors (with or without the filter) and the Tweener system. The terms SWF1, SWOF1, DWF1, and DWO1 represent the air temperature errors of the HMP45C sensors in the first month and the terms SWF2, SWOF2, DWF2, and DWO2 represent corresponding measurements during the second month (after switching the HMP45C sensors). Similarly, the air temperature error produced in the RMY system was defined as the difference between the RMY system and the Tweener system (i.e., RMY1 for period 1 and RMY2 for period 2).

Three methods were used in the data analysis. One was a time series data decomposition to remove noise from the original air temperature errors (e.g., SWF1) using orthogonal wavelet transform (Misiti et al., 1996; Torrence and Compo, 1998). The second method was a statistical analysis to describe the air temperature errors in terms of the three-sigma errors, rather than the standard deviation or probable error terminologies (Barry, 1978). The third method was a time series data spectral analysis method (Bath, 1974).

Data from instruments and sensors usually contain random noise. Since the HMP45C and RMY temperature sensors were taking average measurements, the air temperature errors caused by random noise, especially in high-frequency components, were not contributed by the radiation shields (single or double) or the HMP45C sensors (with filter or without filter). We can assume that both the HMP45C temperature sensor and the Gill shield acted as lowpass filters. The wavelet de-noising approach was a data filtering method to retrieve useful information, which was defined as air temperature trends or patterns (low-frequency components in time scales: minutes, hours, and days) in time series data for this study. The wavelet de-noising allows us to separate all high-frequency noise and retain the variations of lower frequency components, which are contributed from the radiation shields and the HMP45C sensors with or without the filter, consistent with the focus of this study. The specific wavelet transform method selected was a multiple-level

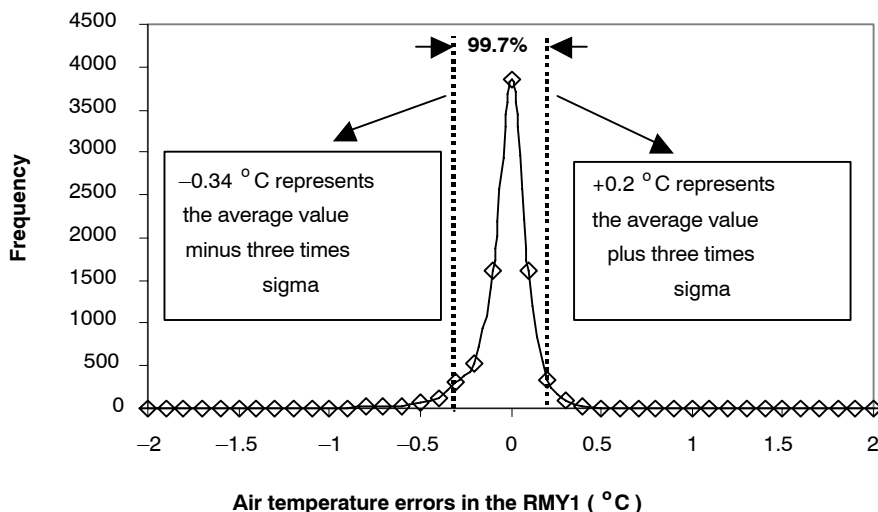


Figure 2. Histogram of the air temperature errors and three-sigma errors (standard deviation, σ) in the RMY system during the first month.

decomposition. The optimal wavelet basis function and level of wavelet decomposition were chosen in terms of a minimum entropy criterion (Coifman and Wickerhauser, 1992; Misiti et al., 1996). In this study, we chose the Daubechies wavelet (dbN, where N = 3 was selected) and four levels of decomposition to remove the noise components in the time series of air temperature errors.

Measurement errors are often described statistically, and air temperature errors for calibrated sensors may be distributed about zero in a quasi-normal fashion. Figure 2 presents the error distributions for the RMY1 system in this study ($T_{RMY1} - T_{Reference}$). The area between -3σ and $+3\sigma$ on the frequency curve contains about 99.7% of the total area,

which means only 1 chance in 370 of lying beyond. This compares to the probable error (50% certainty, 1 chance in 2), standard deviation error (68.3% certainty, 1 chance in 3), and two-sigma error (95.5% certainty, 1 chance in 20). Thus, the three-sigma error is more “practical and reasonable” from the perspective of representing “maximum error” (accuracy).

The power spectral analysis is a method based on the Fourier transform to extract useful information related to corresponding frequencies from a signal. Using the Fourier transform, the power spectral density of a signal simply finds the discrete-time Fourier transform of the samples of the signal and takes the magnitude squared of the result. The power spectral density reveals the degree of contribution to

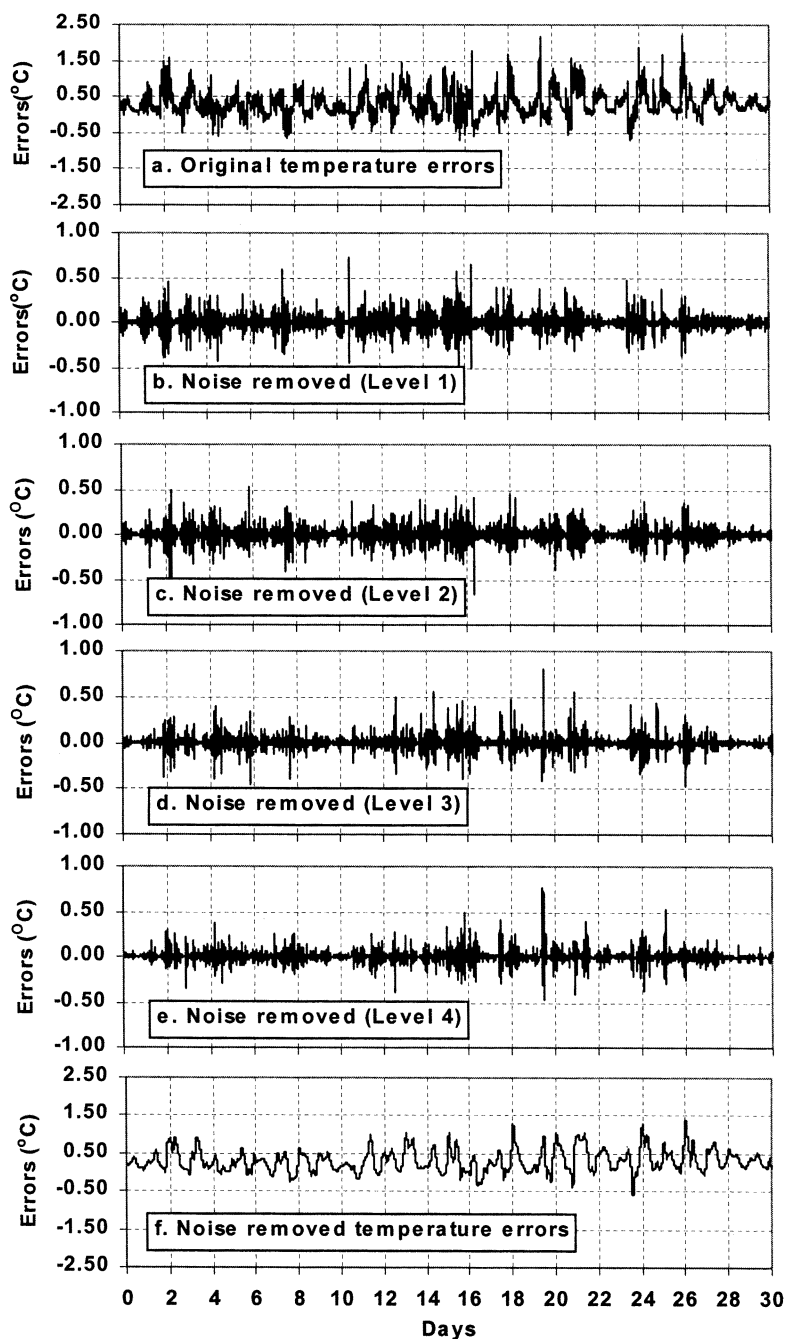


Figure 3. Illustration of noise removal of air temperature errors in measurements. The original signal of air temperature errors illustrated here is from the SWF1.

the total air temperature error from variations at particular frequencies. We scaled the magnitude squared of the Fourier transform by the square of the norm of the non-rectangular window applied to the signal (a length 1024 Hanning window was used in this study) to ensure that the computation is asymptotically unbiased (Bath, 1974).

RESULTS AND DISCUSSION

The process of applying the wavelet transform to remove noise from the original air temperature errors in the HMP45C system and the RMY system is illustrated in figure 3. The original air temperature errors of SWF1 demonstrated significant noise in the signal (fig. 3a). The frequency of noise components removed from level 1 to level 4 is decreased at frequencies 10, 20, 40, and 80 min per cycle in the octave scale. The information content in time series data retained the same entropy when the noise removal was up to the fourth level (i.e., the frequency at 80 min per cycle). The high-frequency noise fluctuated more strongly during the daytime, especially at midday (figs. 3b to 3e) due to the solar radiation effects, including short-term cloud cover, on the air temperature measurements in the Gill radiation shield. The air temperature error after removing high-frequency noise is

much “cleaner” and represents the lower frequency components needed to detect the differences between the single Gill shield and the double Gill shield, and between the HMP45C sensors with and without the filter.

After removing the noise, the time series data were displayed (figs. 4 to 6) with statistical results for the two experimental periods. During both months (figs. 4 and 5), all combinations of the HMP45C sensors and Gill shield represent positive average air temperature errors. The difference between the RMY air temperature system and the Tweener system were centered about zero (fig. 6). If we assume that there was no systematic error during the calibration of the HMP45C, then the introduction of both the filter on the HMP45C sensor and the Gill shield should contribute a positive (heating) source to the air temperature measurement on average.

The values of average air temperature errors in SWF1 and DWF1 were more than 0.1°C higher than the values in SWOF1 and DWO1 on average (fig. 4). From the view of three-sigma errors, the HMP45C sensor with the filter had much more variation than the sensor without the filter. The air temperature errors in the HMP45C sensor with the filter could possibly reach more than 1.0°C in the positive direction, which suggests that the maximum air temperature

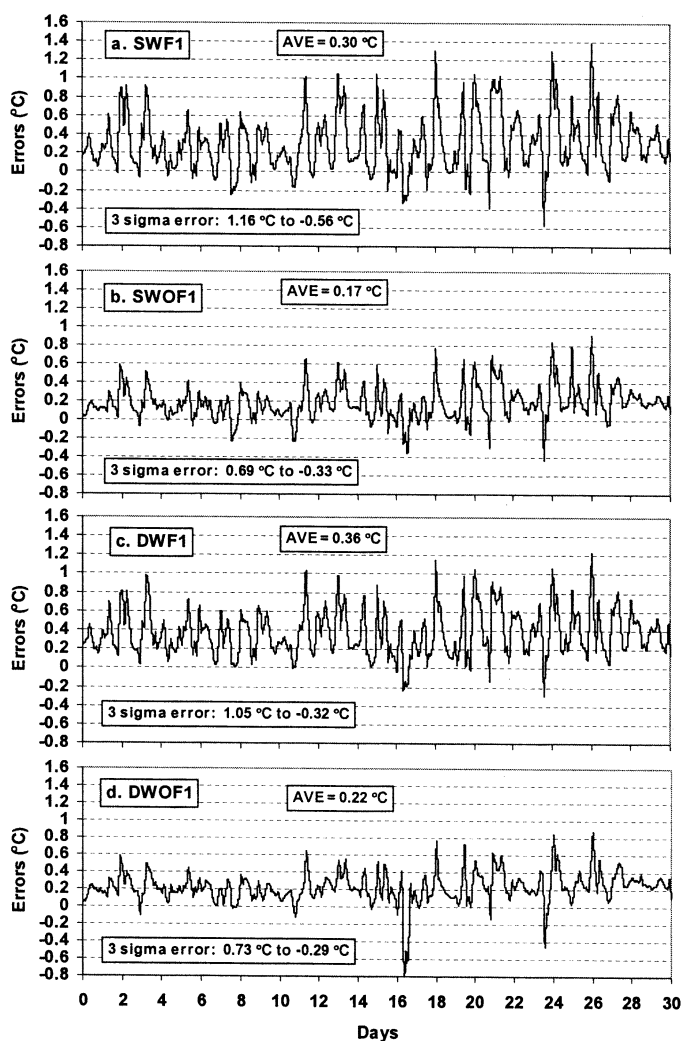


Figure 4. Time series of air temperature errors and statistical values for the HMP45C sensors during the first month.

records taken with the filter may reach one degree higher than without the filter. The HMP45C sensor without the filter improved the accuracy in both single and double Gill shields.

Turning our attention to the difference between the single shield and the double shield, we find that the double Gill shield was less accurate compared to the single Gill shield (fig. 4). Thus, the results did not support the hypothesis that heat conduction along the partially exposed housing of the HMP45C sensor is significant. One explanation for this result might be that the sensing elements of the HMP45C sensors were in different relative locations inside the shields. Thus, the air speed past the sensing element might result in less ventilation for the double shield. In fact, vertical profiles of horizontal wind speed do vary with height for the single Gill shield (Lin, 1999; Lin et al., 2001a). It is also possible that the partially exposed body of the HMP45C sensor is, on average, a cold source that withdraws heat from the head of the HMP45C inside the Gill shield during nighttime because the

lower housing is totally exposed outside the shield and experiences relatively larger air speed (ambient wind speed) to enhance its convection heat exchange.

In figure 5 we find similar results for the differences between the single shield and double shield, and between the HMP45C with the filter and without the filter, after the HMP45C sensors were switched. Therefore, we can state that there was no systematic error inherent in the HMP45C sensors in our study. Similarly, in the second period, the variation of air temperature errors in the HMP45C with the filter was higher than that in the HMP45C without the filter. The double shield again did not perform as well as the single shield (fig. 5). Results indicate that the range of three-sigma errors (difference between upper and lower bounds) in the HMP45C with the air filter was about $+0.4^{\circ}\text{C}$ to $+0.7^{\circ}\text{C}$ larger than that in the HMP45C without the air filter (figs. 4 and 5).

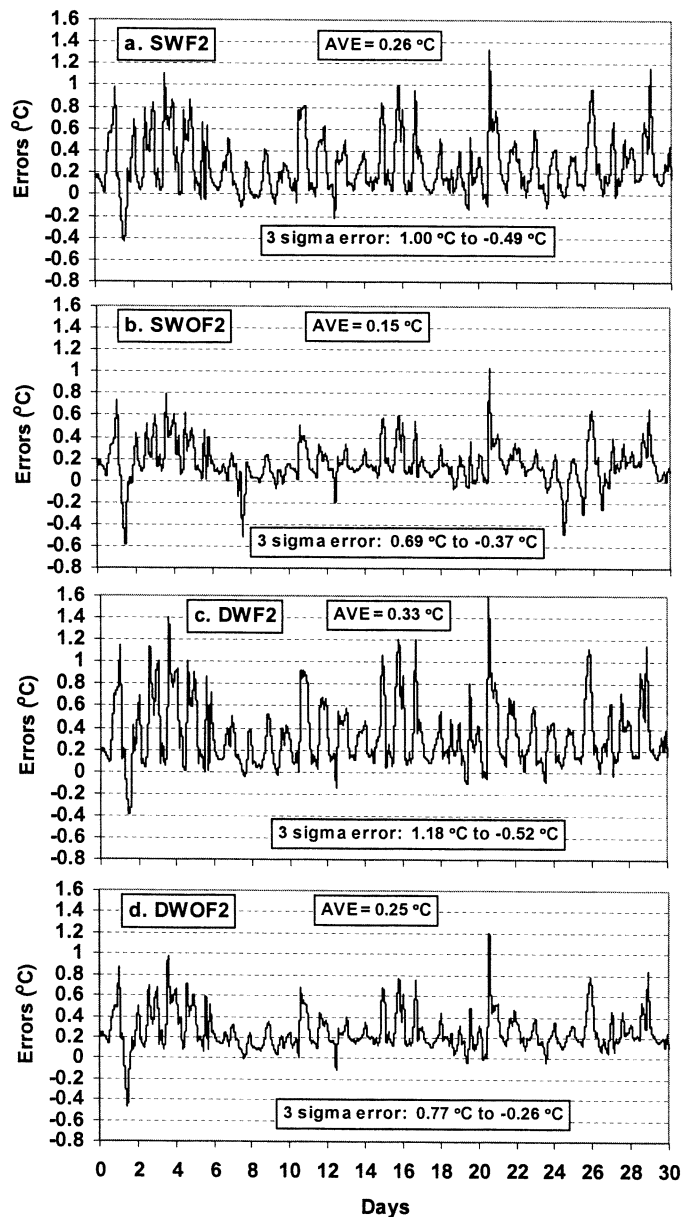


Figure 5. Time series of air temperature errors and statistical values for the HMP45C sensors during the second month.

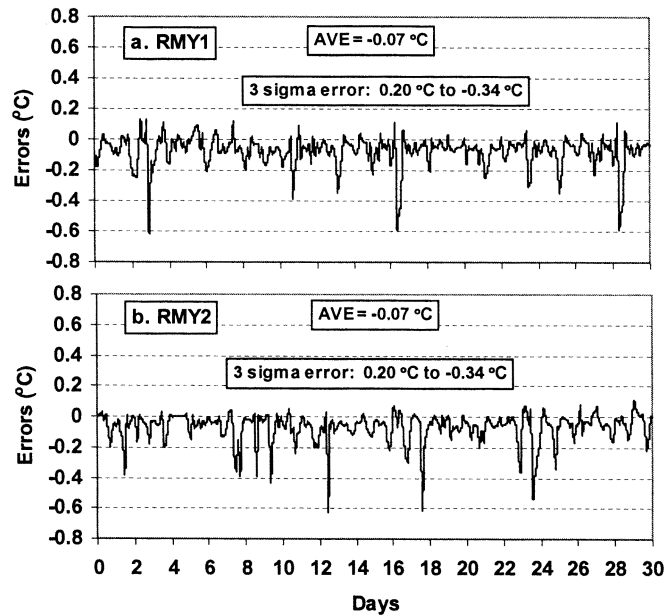


Figure 6. Time series of air temperature errors and statistical values for the RMY temperature system.

The results in figure 6 show relatively small air temperature errors in the RMY system. The average air temperature errors (-0.07°C) and three-sigma errors ($+0.20^{\circ}\text{C}$ to -0.34°C) were identical for the two scenarios. This result suggests that the RMY air temperature measurement system, with the R. M. Young 43347 temperature probe, is an excellent thermometer in the field. Another interesting point in the time series of the air temperature errors of the RMY system is that all relatively large variations were slightly negative, which suggests that the RMY system provided excellent filtering of solar radiation (a heating source) compared to the filtering of infrared radiation (a cooling source) during nighttime, with respect to air temperature errors (Hubbard et al., 2001).

Figures 7, 8, and 9 show the average power spectral density of the air temperature errors for each system. The unit of power spectral density in this case is $(^{\circ}\text{C})^2$ per frequency, which indicates the energy distribution of the air temperature error at each frequency component (Bath, 1974). The period (days per cycle) was plotted on the horizontal axis instead of frequencies (figs. 7 and 8). One pronounced peak at the period of one day per cycle was found for all cases involving the measurements of the HMP45C sensor with the Gill shield. However, the magnitudes in the SWF1, SWF2, DWF1, and DWF2 systems were much higher than in SWOF1, SWOF2, DWOFF1, and DWOFF2. This suggests that the air temperature errors in the HMP45C sensor with the filter led to much higher variations at the frequency of one day per cycle compared to the HMP45C without the filter. For the comparison between the single shield and the double shield, there were no obvious differences (figs. 7 and 8).

Results from the spectral analysis were consistent with the above statistical analysis in the time domain. This suggests that the solar radiation driving force, partially blocked by the radiation shields, still plays an important role in the air temperature measurement and contributes to this frequency of one day per cycle. However, the HMP45C sensors without the filter had a decreased amplitude of the power spectral density of the air temperature errors at the frequency of one

day per cycle. In addition, it seems that there was another peak around 6 to 7 days per cycle in each case (figs. 7 and 8), especially for the HMP45C sensor without the filter (e.g., DWOF1, SWOF2, and DWOFF2). This may be associated with synoptic-scale storms or the changes of air masses at our experimental site, which occur on a 5 to 10 day time scale. The stronger winds associated with the passage of low-pressure systems may cause non-ventilated shields to track the aspirated shield more closely for a few days, while lower winds associated with high-pressure systems may cause the readings to deviate during intervening days.

When keeping the same power spectral density scales for the RMY system, the pronounced peaks at the frequency of one day per cycle still exist, but they were very small (fig. 9). Figure 9 shows that the spectral analysis was consistent with the earlier statistical analysis.

CONCLUSION

Both statistical and spectral analysis indicate that the average air temperature errors and the variations of air temperature errors are smaller in the HMP45C sensors with the air filter removed compared to the standard HMP45C sensor (with the air filter). The accuracy of the monthly average air temperature can improve at least 0.1°C , and the ranges of three-sigma errors can be decreased by 0.4°C to 0.7°C for an HMP45C without the air filter. In addition, the air temperature errors measured in the HMP45C sensor with the filter could possibly reach more than 1.0°C in the positive direction and more than about 0.3°C to 0.5°C in the negative direction, which suggests that the maximum and minimum air temperature records taken with the air filter may reach one degree higher and about 0.3°C to 0.5°C lower than without the air filter, respectively. Therefore, for air temperature measurement, the design of the HMP45C sensor with an air filter is not optimal. Even so, the filter may be a happy compromise in "dirty" environments, where contaminants could cause even larger problems. In the design of the HMP45C sensor, the air temperature probe can be removed

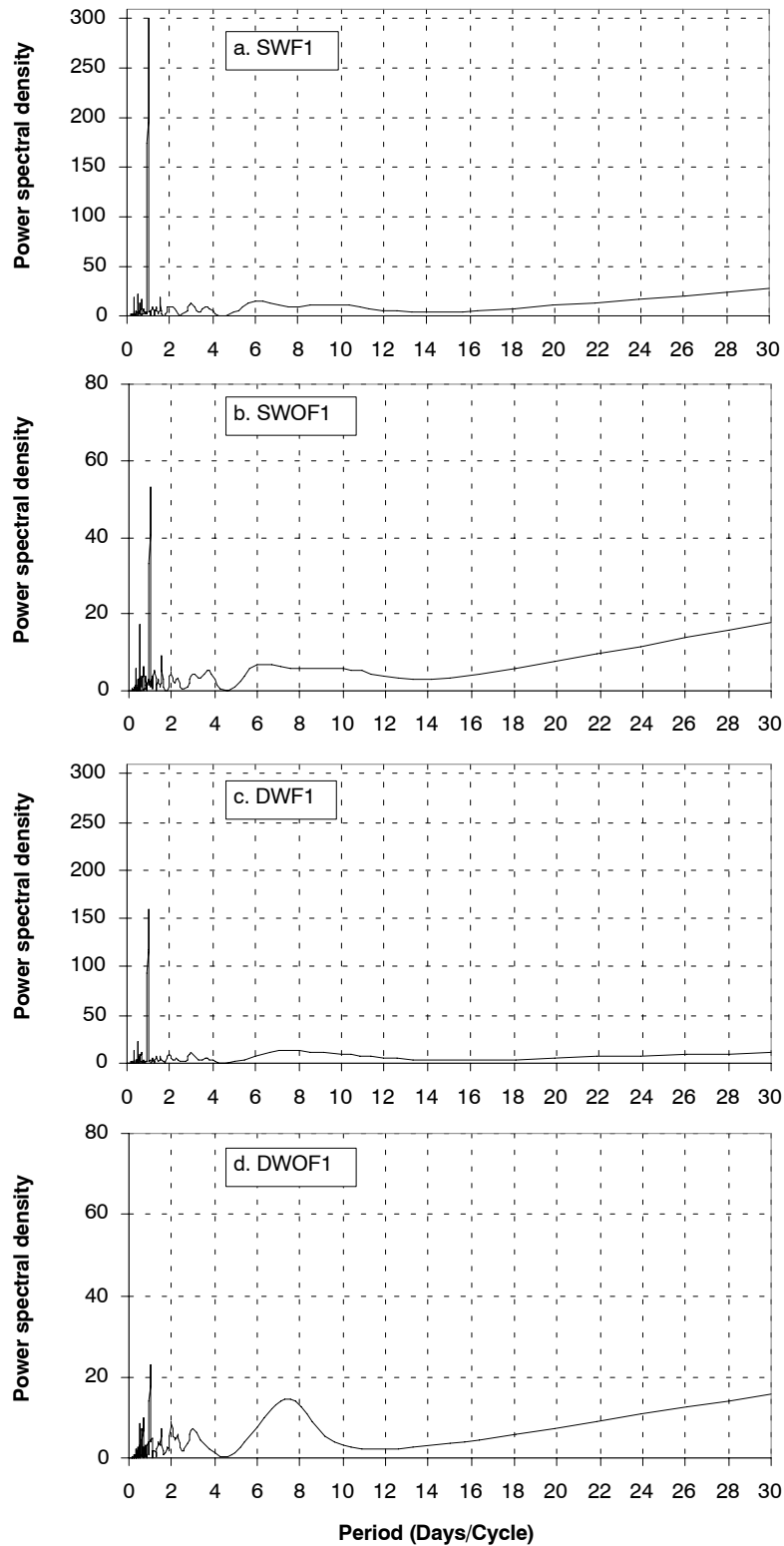


Figure 7. Average power spectral density of the air temperature errors for the HMP45C sensors during the first month.

from the air filter by using an appropriate sheath, but the HUMICAP® 180 capacitive probe cannot be removed from the air filter because it would lose its protection against chemical containment errors.

The double Gill shield did not perform better than the single Gill shield. The hypothesized conduction of heat along the exposed housing of the HMP45C sensor was not

significant in this study. Instead, the conduction heat sink at the exposed end of the HMP45C may dominate the heat transport on average. Spectrally, the major component contributing to air temperature errors using the HMP45C sensor (with an air filter) in the Gill shield was the frequency of one day per cycle.

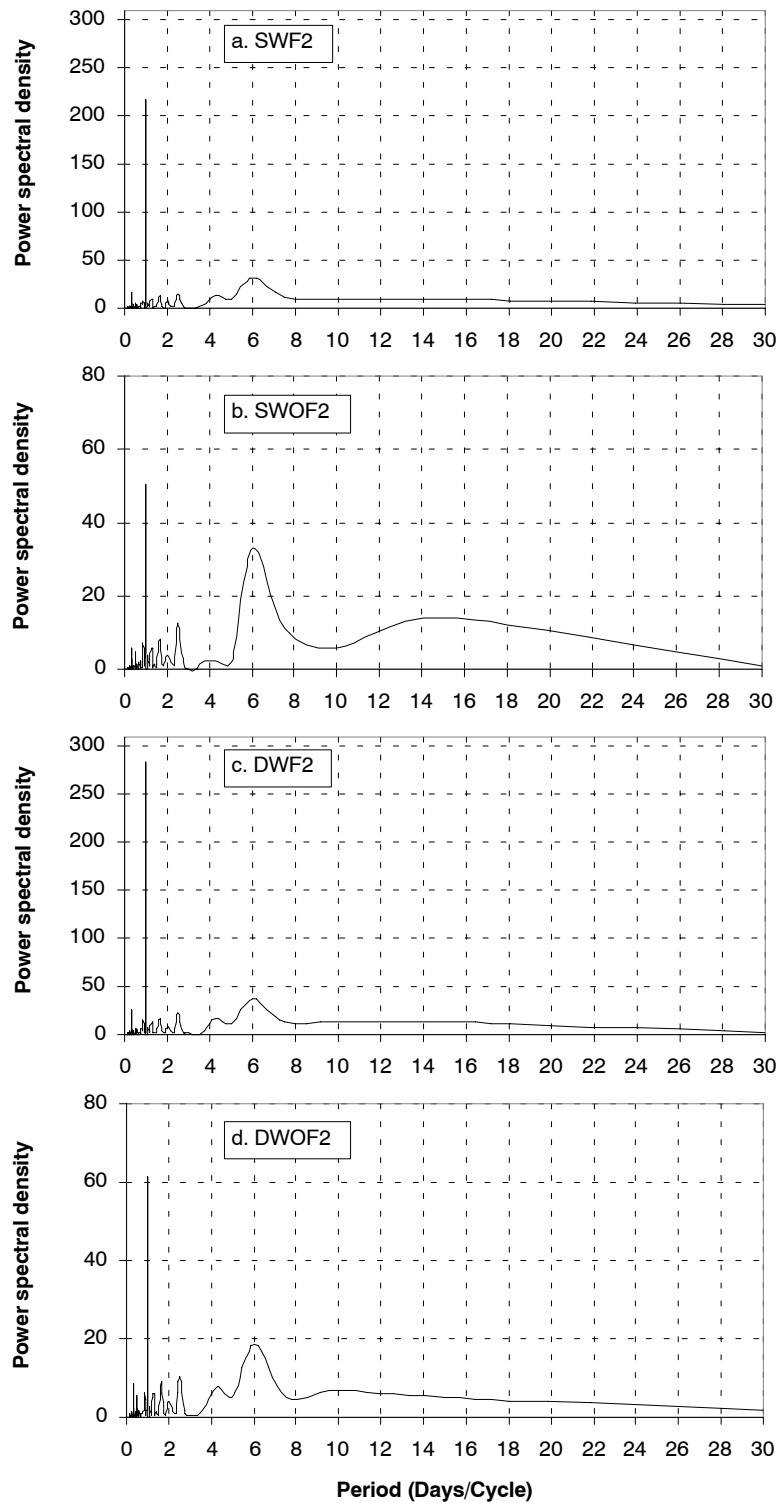


Figure 8. Average power spectral density of the air temperature errors for the HMP45C sensors during the second month.

The R. M. Young 43347 temperature probe with the R. M. Young 43408 aspirated radiation shield proved to be an accurate thermometer system compared to the thermometer composed of a precision industrial PRT probe and a Tween thermometer recorder. The effect of environmental effects of the R. M. Young system in the field was much less than the effects on air temperature in the other shield systems. The RMY system reached field accuracies around $+0.2^{\circ}\text{C}$ to -0.34°C with -0.07°C error on monthly average.

ACKNOWLEDGEMENTS

We appreciate the many thoughtful discussions and insights of Bertrand D. Tanner, Vice President of Campbell Scientific, Inc., on the air temperature measurement errors. We also appreciate the valuable comments and suggestions of Dr. David Jones and Dr. Qi Steve Hu. Support for this study was provided by the High Plains Regional Climate Center at the University of Nebraska–Lincoln.

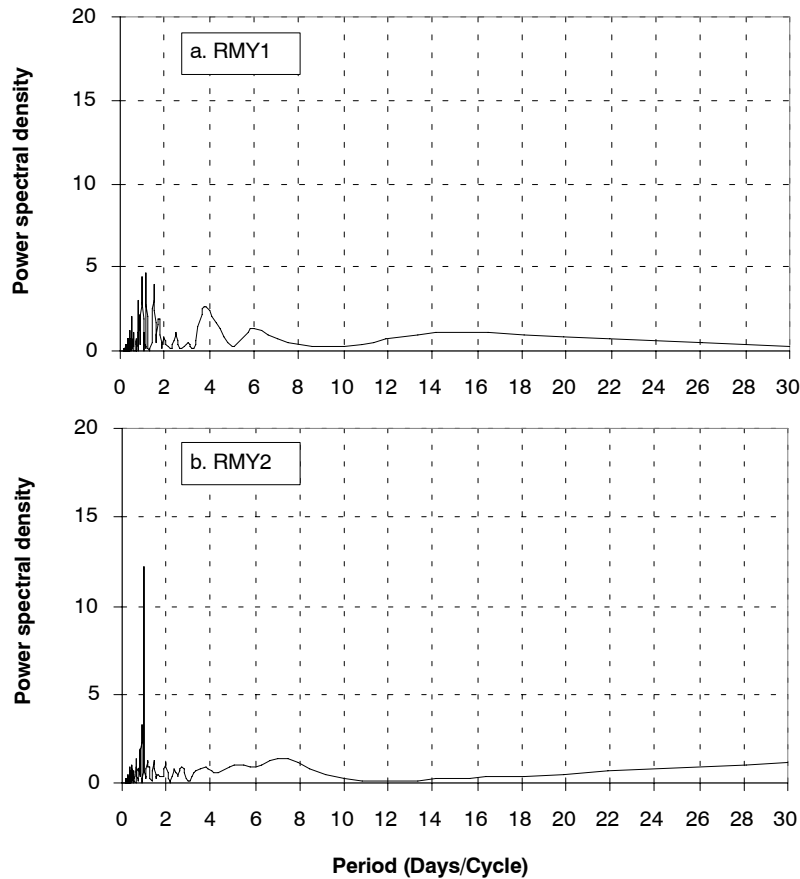


Figure 9. Average power spectral density of the air temperature errors for the RMY system.

REFERENCES

- Barry, B. 1978. *Errors in Practical Measurement in Science, Engineering, and Technology*. New York, N.Y.: John Wiley and Sons.
- Bath, M. 1974. *Development in Solid Earth Geophysics 7: Spectral Analysis in Geophysics*. New York, N.Y.: Elsevier Scientific.
- Brock, F. V., S. R. Semmer, and C. Jirak. 1995. Passive solar radiation shields: Wind tunnel testing. In *Ninth Symp. on Meteorological Observations and Instruments*, P1.3: 179–183. Boston, Mass.: American Meteorological Society.
- Coifman, R. R., and M. V. Wickerhauser. 1992. Entropy-based algorithms for best basis selection. *IEEE Trans. Information Theory* 38(2): 713–718.
- Hubbard, K. G., X. Lin, and E. A. Walter–Shea. 2001. The effectiveness of the ASOS, MMTs, Gill, and CRS air temperature radiation shields. *J. Atmos. Oceanic Tech.* 18(6): 851–864.
- Lin, X. 1999. Microclimate inside air temperature radiation shields. PhD diss. Lincoln, Nebraska: University of Nebraska.
- Lin, X., K. G. Hubbard, and G. E. Meyer. 2001a. Air flow characteristics of commonly used temperature radiation shields. *J. Atmos. Oceanic Tech.* 18(3): 329–339.
- Lin, X., K. G. Hubbard, and E. A. Walter–Shea. 2001b. Radiation loading model for evaluating air temperature errors with a non-aspirated radiation shield. *Trans. ASAE* 44(5): 1299–1306.
- Misiti, M., Y. Misiti, G. Oppenheim, and J. M. Poggi. 1996. Wavelet toolbox for use with MATLAB. *User's Guide Version 1*. Natick, Mass.: The MathWorks, Inc.
- Torrence, C., and G. P. Compo. 1998. A practical guide to wavelet analysis. *Bull. American Meteorological Society* 79(1): 61–78.